Poster Number:
T31C-0314

Magnetotelluric Evidence for Asymmetric Simple Shear Extension and Lithospheric Thinning in South China

Shan Xu[1], Martyn Unsworth[2], Xiangyun Hu[1], Walter Mooney[3]

[1]China University of Geosciences, Wuhan, Hubei, China, shanxu0919@gmail.com
[2]University of Alberta, Edmonton, Alberta, Canada
[3]USGS, Menlo Park, USA

1. Introduction

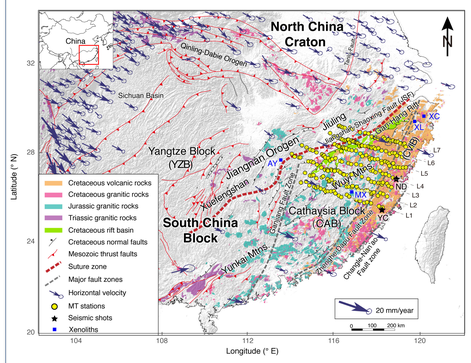

Figure 1. Topography and simplified tectonic map of South China

Extension can cause thinning of the continental lithosphere, resulting in either narrow or wide rifts, or even, continental breakup (Buck, 1991). The South China Block (SCB) is a unique locality as it has an intact cratonic core in the west (the Yangtze Block) and a rifted continental margin in the east (the Cathaysia Block), with widespread normal faults and rift basins interposed by bimodal rhyolite-basalt volcanics, mafic and felsic dyke swarms, shoshonites, extensional domes and alkaline rocks. These features constitute a type example of a wide rift in Southeast China, comparable to the Basin and Range Province in North America (Gilder et al., 1991). However, the actual mechanism of extension in the South China rift system remains enigmatic.

Two end member models have been proposed to interpret the driving forces responsible for lithospheric extension:

(a) pure shear extension, characterized by symmetrically deforming brittle upper lithosphere over a ductile lower lithosphere (Mckenzie, 1978);

(b) simple shear extension, featuring asymmetrical thinning across a low-angle detachment that divides the lithosphere into upper and lower plates (Wernicke, 1984).

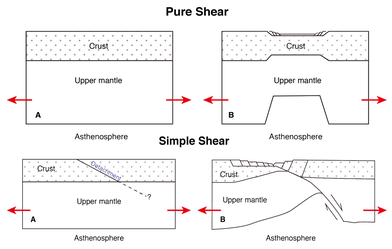

Figure 2. Two main modes of extension

2. 3-D Inversion results

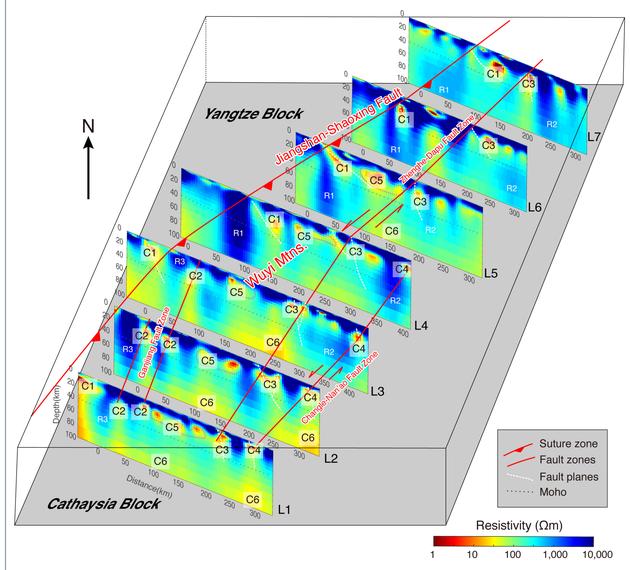

Figure 3. Three-dimensional (3-D) resistivity model projected on the seven profiles.

MT array data were collected at 225 stations along seven survey lines, with an average station spacing of 10 km and line spacing of 50 km (Figure 1). We use three-dimensional (3-D) inversion schemes (ModEM, Egbert & Kelbert, 2012; Kelbert et al., 2014) to image the lithospheric resistivity structure.

The upper crust is dominated by high resistivity (>1,000 Ωm), interposed with low resistivity features (~10 Ωm) mainly along the JSF and in the sedimentary cover (Figure 3 and Figure 4a). The middle crust (5–20 km) exhibits widespread NE-trending highly conductive stripes, interspaced with resistive anomalies. One conductive stripe appears as an ENE-trending anomaly, which is labeled C1 in Figure 3 and Figure 4b, and is coincident with the JSF that marks the boundary between the Yangtze and Cathaysia Blocks. This conductive feature narrows in the brittle upper crust and dips southeastwards at 30–45° on profiles 4 and 5 (Figure 3). Underlying C1, a high resistivity (> 1,000 Ωm) region R1 (Figures 3 and 4), extends from the Yangtze Block and dips southeastwards beneath the Cathaysia Block to a depth over 100 km.

The mantle is highly resistive beneath the Yangtze Block in the depth range of 70–100 km (Figures 4c and 4d). A significant southward decrease of resistivity in the mantle occurs from the JSF and is evidenced by intermediate to conductive mantle in the Cathaysia Block. One prominent feature is that C6 forms a conductive dome beneath the central Wuyi Mountains (Figures 4c and 4d), with the top rising to a depth of ~70 km.

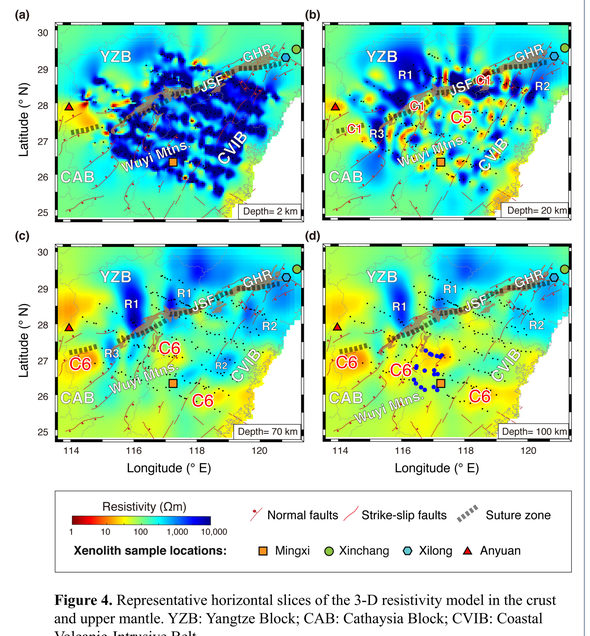

Figure 4. Representative horizontal slices of the 3-D resistivity model in the crust and upper mantle. YZB: Yangtze Block; CAB: Cathaysia Block; CVIB: Coastal Volcanic-Intrusive Belt

3. Discussion

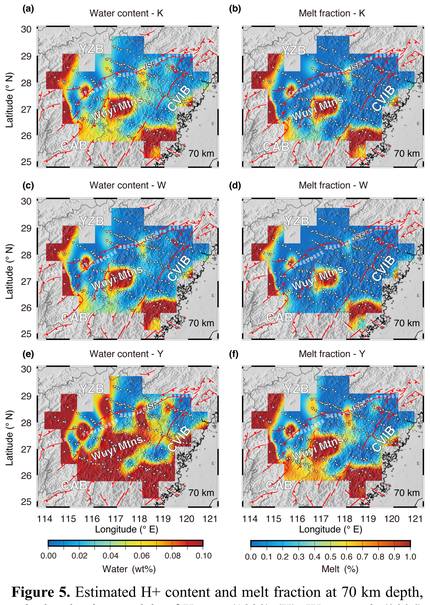

Figure 5. Estimated H+ content and melt fraction at 70 km depth, calculated using models of Karato (1990) (K), Wang et al. (2006) (W) and Yoshino et al. (2009) (Y), respectively.

The H+ content and melt fraction at 70 km (Figure 5) were calculated with resistivity and xenolith derived geotherm based on three published studies (Karato, 1990; Wang et al., 2006; Yoshino et al., 2009). Generally, the regions of water and melt concentration predicted by the three models have the same location, while possessing different values. Elevated water content is observed beneath the JSF, the central Wuyi Mountains and the southern CVIB (Figures 5a, c and e). The water content and melt distribution predicted by Karato (1990) (Figure 5a) and Wang et al. (2006) (Figure 5c) are almost the same. In contrast, Yoshino et al. (2009) predicts more water (Figure 5e) and requires more melt (Figures 5f) to explain the resistivity. Regardless of the different values of the three models, the water distribution indicates that the southern part of the region is more hydrated compared to the northern part, which implies that the lithosphere in the southern part is less viscous and weaker, as both water and partial melt reduces the mantle viscosity. As estimated from the measured low resistivity, the water content is up to 0.1 wt% and melt fraction is up to 1 % at 70 km depth beneath the central Wuyi Mountains.

The Gan-Hang Rift developed primarily along the Jiangshan-Shaoxing Fault (Figure 6), trending ~450 km in a NE-SW direction. Strong topographic asymmetry exists across the Gan-Hang Rift, manifested by elevations of 1,000 m to the east of the rift but lower than 200 m to the west (Figure 6a). Apart from the SE-dipping JSF, normal faults are confined to the eastern shoulder of the rift (Figure 1). In addition, almost all the Early Cretaceous volcanism is observed to the east of the rift (Figure 1). In our study area, the thinning of the crust and lithospheric mantle is horizontally non-uniform, with the most thinning occurring beneath the Wuyi Mountains. To the east of the Gan-Hang Rift, the topography reaches a maximum elevation on the Wuyi Mountains, with a prominent decrease of the associated Bouguer gravity anomaly (Figure 6a). All these features indicate an asymmetric mode of rifting consistent with simple shear extension (Wernicke, 1984) along the trans-lithospheric fossil suture (JSF), which seems to be a low-angle detachment.

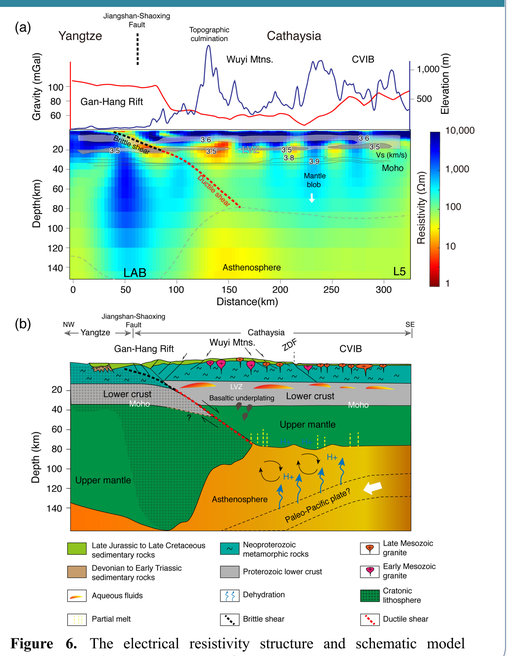

Figure 6. The electrical resistivity structure and schematic model showing the lithospheric structure of Southeast China.

4. Conclusions

Our measurements show that the lithosphere of the SCB exhibits a major change across the JSF, with a resistive and thick lithosphere beneath the Yangtze Block to the northwest and a conductive and thinner lithosphere beneath the Cathaysia Block to the southeast. The distinct lithospheric structure across the JSF shows the importance of an ancient suture zone on the pattern of much younger lithospheric deformation and rifting. While being a Neoproterozoic suture zone documenting the collision of the Yangtze and Cathaysia Blocks, the present-day southeastward dipping JSF was reactivated largely by the Triassic intracontinental orogeny. It acted as a trans-lithospheric low angle detachment fault and enabled asymmetric simple shear extension and rifting during the Mesozoic. Water content of up to 0.1 wt% and melt fraction of up to 1% are estimated at 70 km depth beneath the central Wuyi Mountains, indicative of a hydration process likely resulting from the Paleo-Pacific subduction. The addition of water is hypothesized to cause the weakening and delamination of the lithospheric root of the Wuyi Mountains, which created space for asthenosphere upwelling.

5. Reference

Buck, W. R. (1991). Models of continental lithospheric extension. Journal of Geophysical Research, 96(B12), 20161–20178..

Egbert, G. D., & Kelbert, A. (2012). Computational recipes for electromagnetic inverse problems. Geophysical Journal International, 189(1), 251–267.

Gilder, S. A., Keller, G. R., Luo, M., & Goodell, P. C. (1991). Eastern Asia and the western Pacific timing and spatial distribution of rifting in China. Tectonophysics, 197(2), 225–243.

Karato, S. I. (1990). The role of hydrogen in the electrical conductivity of the upper mantle. Nature, 347, 272.

McKenzie, D. A. N. (1978). Some remarks on the development of sedimentary basins. Earth and Planetary Science Letters, 40, 25–32.

Wang, D., Mookherjee, M., Xu, Y., & Karato, S. (2006). The effect of water on the electrical conductivity of olivine. Nature, 443(7114), 977–980.

Wernicke, B. (1984). Uniform-sense normal simple shear of the continental lithosphere. Canada Journal of Earth Sciences, 22, 108–125.

Yoshino, T., Matsuzaki, T., Shatskiy, A., & Katsura, T. (2009). The effect of water on the electrical conductivity of olivine aggregates and its implications for the electrical structure of the upper mantle. Earth and Planetary Science Letters, 288(1–2), 291–300.